Thermal and Mechanical Performance of a Carbon/Carbon Composite Spacecraft Radiator

Jonathan Kuhn, Steve Benner, Dan Butler, and Eric Silk

NASA/Goddard Space Flight Center
Greenbelt, MD 20771

ABSTRACT

Carbon-carbon composite materials offer greater thermal efficiency, stiffness to weight ratio, tailorability, and dimensional stability than aluminum. These lightweight thermal materials could significantly reduce the overall costs associated with satellite thermal control and weight. However, the high cost and long lead-time for carbon-carbon manufacture have limited their widespread usage. Consequently, an informal partnership between government and industrial personnel called the Carbon-Carbon Spacecraft Radiator Partnership (CSRP) was created to foster carbon-carbon composite use for thermally and structurally demanding space radiator applications. The first CSRP flight opportunity is on the New Millennium Program (NMP) Earth Orbiter-1 (EO-1) spacecraft, scheduled for launch in late 1999. For EO-1, the CSRP designed and fabricated a Carbon-Carbon Radiator (CCR) with carbon-carbon facesheets and aluminum honeycomb core, which will also serve as a structural shear panel.

While carbon-carbon is an ideal thermal candidate for spacecraft radiators, in practice there are technical challenges that may compromise performance. In this work, the thermal and mechanical performance of the EO-1 CCR is assessed by analysis and testing. Both thermal and mechanical analyses were conducted to predict the radiator response to anticipated launch and on-orbit loads. The thermal model developed was based on thermal balance test conditions. The thermal analysis was performed using SINDA version 4.0. Structural finite element modeling and analysis were performed using SDRC/I-DEAS and UAI/NASTRAN, respectively. In addition, the CCR was subjected to flight qualification thermal/vacuum and vibration tests. The panel meets or exceeds the requirements for space flight and demonstrates promise for future satellite missions.

Keywords: Spacecraft Radiator, Carbon-Carbon Composite, Thermal/Vacuum Testing, Vibration Testing, Thermal Modeling, Structural Modeling, EO-1, and Performance

1. INTRODUCTION

The New Millennium Program (NMP) Earth Orbiter-1 (EO-1) is the spacecraft platform for the Advanced Land Imager (ALI) instrument and will fly in a sun-synchronous orbit 705 kilometers above the Earth. The launch date is scheduled for late 1999 aboard a Delta 7320 Expendable Launch Vehicle (ELV). Though the ALI is the primary instrument aboard the EO-1, the spacecraft will also be used to test a number of new technologies, one of which is the Carbon-Carbon Radiator (CCR) shown in Figure 1. The CCR is a sandwich composite panel with facesheets made of carbon fibers in a carbon matrix. In flight, the panel will be attached to the spacecraft bus, and will support two electronics boxes with a total weight of 58 lb and total heat output of 60W. The panel was built by the Carbon-Carbon Spacecraft Radiator Partnership (CSRP) and delivered to NASA/Goddard Space Flight Center (GSFC) for environmental testing. The spacecraft integrator, Swales Aerospace Inc. (SAI)[1], specified the thermal and mechanical flight requirements for the CCR. During the testing at GSFC, the integrated honeycomb panel was subjected to thermal/vacuum and vibration tests. In support of these tests computer models were developed and correlated as needed to understand the response of the CCR to the respective environments. In this paper, the results of GSFC environmental testing and modeling are presented and used to assess the performance of the CCR design.

The CSRP is an informal partnership established to promote the use of carbon-carbon on spacecraft. CSRP membership includes research engineers and scientists at government and private facilities. The government agencies include the Air Force Research Laboratory's Materials and Manufacturing Directorate and Space Vehicles Directorate, the Naval Surface Warfare Center's Carderock division, NASA Langley Research Center (LaRC), NASA Goddard Space Flight Center (GSFC). Private industry members include TRW, Lockheed Martin Astronautics (LMA), Lockheed Martin Missiles & Space (LMMS), Lockheed Martin Vought Systems (LMVS), Amoco Polymers, Materials Research & Design (MR&D), and BF Goodrich. The CSRP designed and fabricated a radiator panel that could significantly reduce spacecraft weight and thermal control costs and possibly extend their operational lives. The panel was built to demonstrate that carbon-carbon can be a cost efficient choice for radiators that also function as part of the primary spacecraft structure. In this case the radiator is also a shear panel. The panel will be instrumented for on-orbit data. If successful, the new design may dramatically change how radiators are constructed for future spacecraft and could lead to other important cost-reduction applications in space and private industry. Flight and spare panels were built and both were subjected to flight qualification testing. This paper focuses on the results of the actual flight panel.

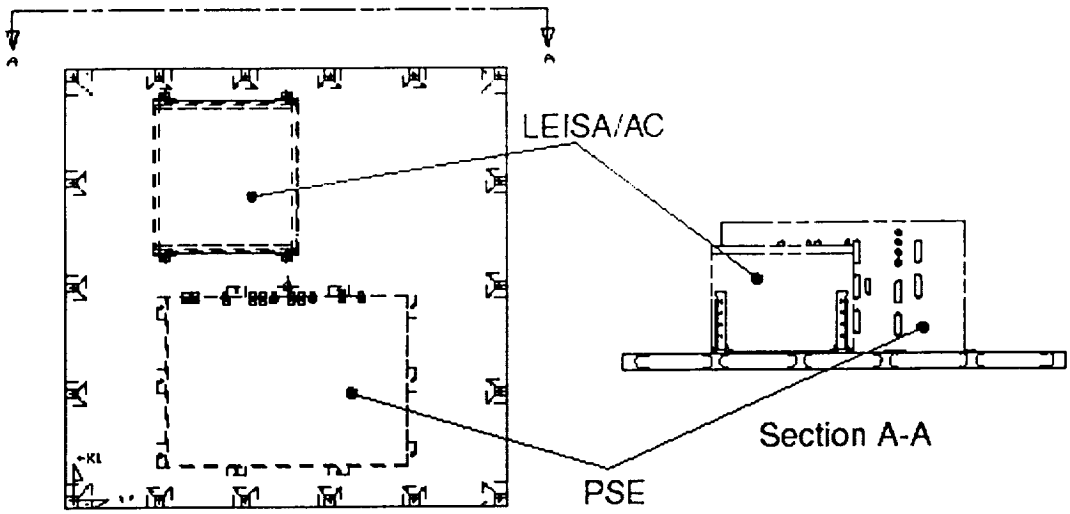

Figure 1: Carbon-Carbon Radiator with Attached Electronics Boxes. (Drawing provided by SAI[1])

Carbon-carbon (C-C) is a special class of composite materials in which both the reinforcing fibers and matrix materials are made of pure carbon. The use of high conductivity fibers in C-C fabrication yields composite materials that have high stiffness and high thermal conductivity. Since C-C density is lower than that of aluminum, significant weight savings may be realized by replacing aluminum panels with such panels. C-C also has an advantage over other high conductivity composite materials in that the thermal conductivity through the thickness is considerably higher. The trend for future satellites is towards higher power density in combination with a reduction in spacecraft size and weight. Since C-C materials also have a markedly higher specific thermal efficiency than aluminum; they offer improved performance for lower volume and mass. They will enable more compact packaging of electronic devices because of their ability to effectively dissipate heat from high power density electronics. Studies have shown that entire heat pipe panels may be replaced by high conductivity C-C for some applications, thus reducing system complexity as well as integration and testing costs. Also, since carbon-carbon is a structural material, it may serve a dual purpose as both a structural and a thermal management material. The material may eventually eliminate the need for thermal doubler plates, which typically add substantial mass to a spacecraft. Finally, because C-C is a composite, its structural and thermal properties are tailorable, thus adding capability and flexibility to spacecraft designs.

Due to high fabrication cost and low interlaminar shear strength, successful application of carbon-carbon composite materials have been limited to non-structural thermal protection and frictional applications. Examples include the space shuttle wing leading edges and aircraft brakes. However, recent advances in carbon-carbon materials fabrication have improved the viability of carbon-carbon for thermally demanding structural applications (see Ref. 2). In an effort to demonstrate the structural potential of carbon-carbon, the CSRP built a structural panel and subjected the sub-components (facesheets and insert regions) as well as the integrated panel to numerous tests. A total of 9 carbon-carbon facesheets were fabricated by BFGoodrich[3]. One facesheet was delivered to LARC for destructive testing. Six facesheets were used to build three honeycomb panels. One integrated panel was delivered to LMA[9] for destructive testing, and two panels (one flight and one backup) were delivered to GSFC for flight qualification testing and performance evaluation. The results of the destructive facesheet tests, which include thermal and mechanical properties, are presented in Refs. 4 and 5, and the results of the panel destructive testing, which include insert pullout testing, are presented in Ref. 5. The results of the testing completed at GSFC are presented in this paper.

Environmental testing of the EO-1 CCR completed at GSFC included thermal and mechanical tests. The thermal testing consisted of three parts. First the radiator underwent four thermal cycles with four-hour soaks at 60°C and -20°C; second, the radiator underwent thermal balance testing for a variety of conditions. And third, survival heaters used to maintain the electronics boxes at 0°C were turned on with five different voltages. Aluminum base plates were designed to simulate the thermal and stiffness properties of the electronics boxes, and were attached to the panel during thermal/vacuum testing. Mechanical testing at GSFC consisted of 18.5 G sine burst tests in each axis accompanied by pre and post low level (0.25 G) sine sweeps across the frequency range of 15-200Hz.

In flight, the CCR, which has a very low CTE, will be attached to the EO-1 aluminium spacecraft bus, which has a high CTE. This may result in substantial stresses as the spacecraft temperature varies from ambient. As such, an aluminum frame was

designed to simulate the stiffness of the spacecraft and attached to the panel during each phase of testing. Mass mock-ups were designed to simulate the inertial properties of the electronics boxes, and were attached to the panel during vibration testing. During the thermal cycle test, the mechanical load induced by the thermal expansion mismatch between the radiator and frame was monitored. Test results showed that the panel successfully met the requirements for the EO-1 mission.

In conjunction with the above environmental testing, thermal and mechanical models were developed at GSFC. The objective of the modeling was to help ensure successful environmental testing, help understand the panel response to anticipated launch and on orbit thermal and mechanical loads, and to verify that the panel meets the flight requirements. Unfortunately, limited time and resources precluded direct comparison of the CCR design with an aluminum baseline. In the following sections, the CCR design is briefly discussed. Subsequently, the thermal modeling and testing details are presented, followed by the thermal results. In a similar fashion the mechanical modeling and testing details are presented, followed by the mechanical results. Finally, the results presented here are used to assess the thermal and mechanical performance of CCR.

2. CARBON-CARBON RADIATOR DESIGN

The primary thermal function of the EO-1 CCR is to radiate heat generated by two electronics boxes to space. These are the Power System Electronics (PSE) box with a power output of 50W and the LEISA/AC box with a power output of 10W. The panel must support the combined weight of the PSE (50-lb) and the LEISA (10-lb) boxes under substantial launch loads. As a structural shear panel, the CCR is required to sustain significant shear loads induced by the spacecraft bus. The CCR must also react potentially significant stresses due to on-orbit thermal variances combined with the CCR/spacecraft Coefficient of Thermal Expansion (CTE) mismatch. Finally, the first mode frequency of the panel and box assembly must exceed 100Hz to avoid resonance during launch. Each of these challenges is addressed by the CCR design.

The CCR design consists of a sandwich panel construction with two 0.022" thick Carbon-Carbon facesheets bonded to 5056 Aluminum Honeycomb 2.1 lb/ft^3. The dimensions of the panel are approximately 28.62" x 28.25" x 1" and the panel weighs approximately 5.5 lb. The panel is attached to the spacecraft through 18 attachment points at the perimeter and supports the two electronics boxes through 14 attachment points on the interior, as shown in Figure 1. Eight (8) additional insert locations are provided for Ground Support Equipment (GSE). The panel is coated with an epoxy encapsulant to prevent particle contamination of sensitive instruments on board EO-1, and to provide additional strength to the panel. In flight, the CCR will have a clear field of view (FOV) to space. The design includes a layer of silver teflon tape on the external side of the panel.

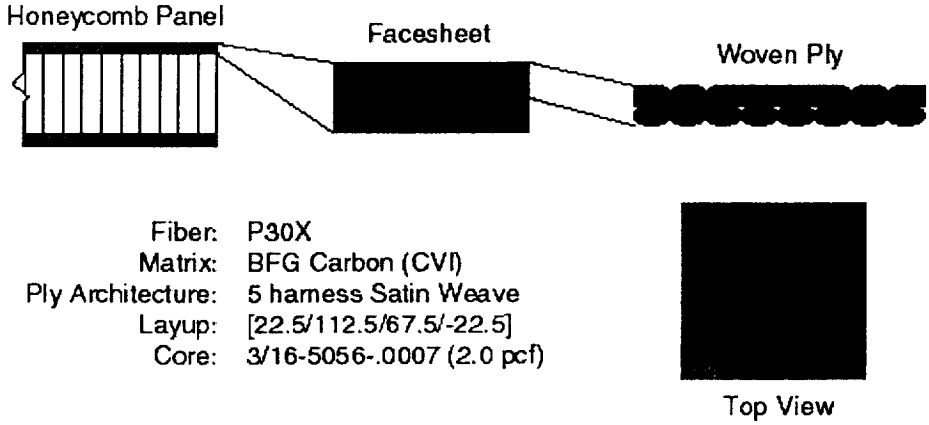

Figure 2: Facesheet Design

The CSRP selected the carbon-carbon facesheet design based on a material trade study completed by MR&D[6]. Each facesheet is comprised of two plies of 5-harness satin weave fabric as shown in Figure 2. The fabric is constructed from P30X carbon fibers and the carbon matrix is introduced by Chemical Vapor Infiltration (CVI). B.F. Goodrich fabricated the facesheets. LMVS[8] designed the perimeter and interior attachment point configurations. The design consists of aluminum inserts bonded to the honeycomb core and facesheets with potting compound as shown in Figure 3. The perimeter insert design used to attach the panel to the spacecraft is shown in Figure 3a. The interior insert design used to attach the electronics boxes is shown in Figure 3b. In both cases, the potted insert design is such that the inserts do not bear directly against the facesheets. Load is transferred through the inserts to the potting compound and into the facesheets and honeycomb core. In this configuration the potting compound effectively acts like an elastic spring between the facesheets and spacecraft frame to relieve thermal expansion mismatch stresses. Clearance through-hole diameters in the perimeter inserts were also specified by SAI to reduce the loads induced by the thermal mismatch. Further details of the design and fabrication of the radiator are presented in Ref. 5.

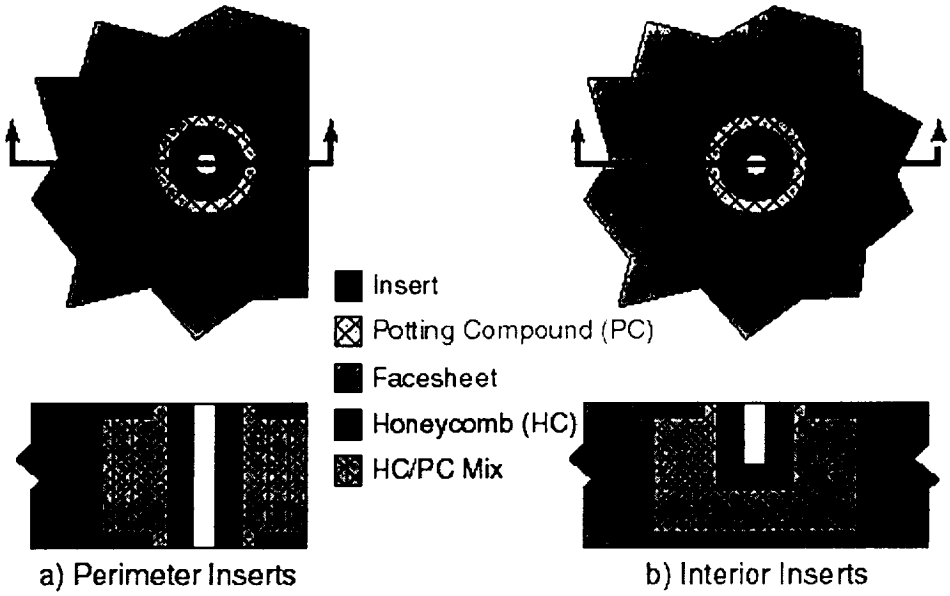

Figure 3: Insert Design

For the purposes of analysis and testing, four configurations of the panel assembly, listed in Table 1, are considered. Finite element models of configurations B and D are shown in Figure 4, and case A is described in more detail in Ref. 5. Case A is the flight configuration, which was modeled to estimate the stiffness of the region of the structure attached to the panel. These results were used to design an aluminum frame that simulates the stiffness of the spacecraft for testing. The aluminum frame is included in the model shown in Figure 4b. Case B was modeled to analyze the mechanical response to launch loads and to compute the first mode frequency of the panel and box assembly. Case C represents the vibration test configuration and was modeled to simulate the test. The thermal/vacuum test set-up matches case D. Because the frame simulates the stiffness of the spacecraft, case D, was used to analyze and test the thermally induced loads. The thermal models and tests presented in Section 3 are based on case D, and the mechanical models and tests presented in Section 4 are based on cases B and C.

Table 1: Analysis and Testing Configurations

Case	Description	Purpose
A.	Panel Attached to Spacecraft with Boxes	• Flight configuration. • Compute effective stiffness of the spacecraft used to design an equivalent aluminum frame for testing.
B.	Panel Attached to Ground with Rigid Boxes Figure 4a	• Analyze launch loads. • Compute mode shapes.
C.	Panel Attached to Frame with Rigid Boxes	• Vibration test configuration. • Compute test mode shapes.
D.	Panel Attached to Frame with Base Plates Figure 4b	• Thermal test configuration. • Analyze thermal loads and thermal response.

3. THERMAL PERFORMANCE

During flight of the EO-1 spacecraft, the CCR will be required to radiate 60 Watts generated by the electronics boxes to space. The assembly will also be subjected to ambient temperature variations in the range of -10° to +50° C, and survival heaters will be used to maintain the electronics boxes above a minimum temperature of 0°C. The panel was designed and tested to 10° C above and below this expected temperature range. Three thermal/vacuum tests were performed to assess the performance of the CCR. First was a thermal cycling test, second a thermal balance test, and third a survival heater test. A thermal model of the thermal balance test was also developed to provide further insight into the thermal response of the radiator. The details of each of these tests are discussed in the next section, which is followed by a description of the thermal model. Subsequently, results from the environmental tests and analysis are presented and compared.

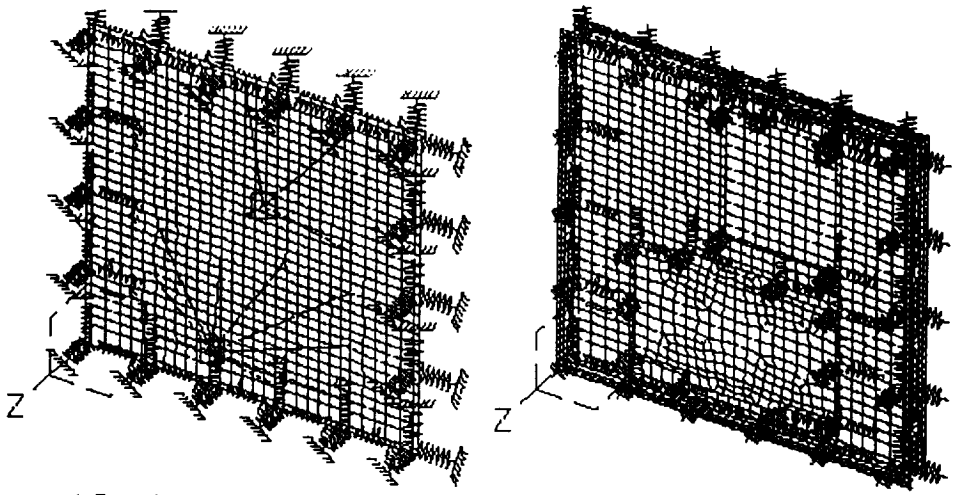

Figure 4: Structural Finite Element Models

1. Thermal/Vacuum Testing

The thermal/vacuum testing was designed to meet the requirements specified by spacecraft integrator, SAI, and to test the performance of the radiator for a variety of conditions. The tests were completed using the cryo-pumped thermal vacuum facility located at GSFC.

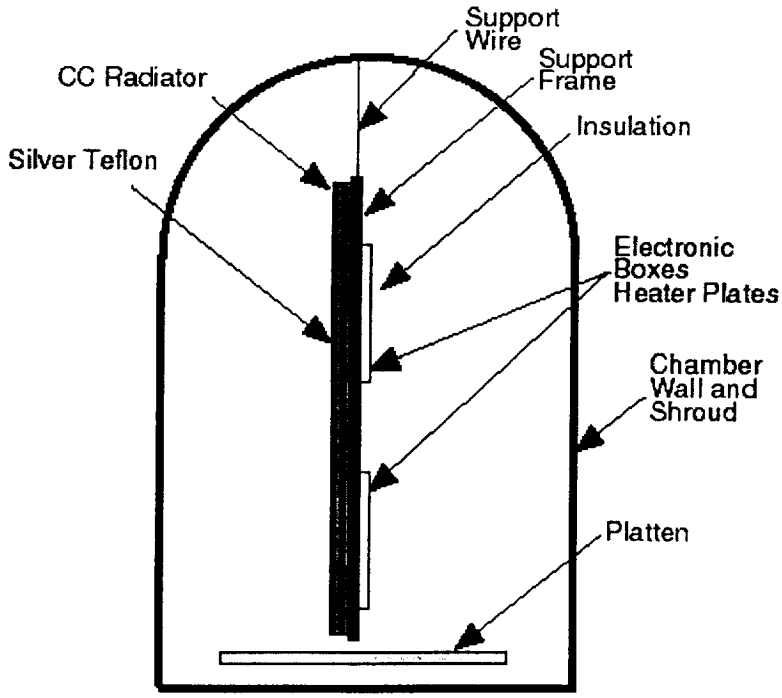

Figure 5: Carbon-Carbon Radiator Thermal Vacuum Setup for the Thermal Balance Test (not to scale)

In the set-up for each thermal test, two aluminum plates were bolted to the radiator to simulate the LEISA and PSE electronics boxes that will be there during flight. A cho-therm thermal interface was placed between the plates and the radiator. The bolts were torqued to the recommended flight values of 38 in-lbs and re-torqued after 24 hours. Heaters capable of generating 50 Watts of power were attached to the PSE plate, and heaters with 30 Watts of power capacity were attached to the LEISA plate. The heaters were attached by two-sided adhesive tape. The power to the two heaters was capable of being adjusted independently. The radiator also had a support frame, which was bolted to the radiator at the spacecraft attachment points. The purpose of the support frame was to simulate the spacecraft interface during environmental testing. The bolts,

which attached the radiator to the support frame, were torqued to the recommended flight values of 38 in-lbs. Two strain gauges were placed on the frame to monitor mechanical forces. The radiator was suspended vertically in the chamber by stainless steel wire. During the thermal balance and survival heater tests, MLI was used to insulate the side with the heaters (see Figure 5). Heater power was monitored continuously by measuring the voltage directly across the heater and by measuring the actual current flowing through the heater. When steady state was reached, the voltage and current were measured and recorded.

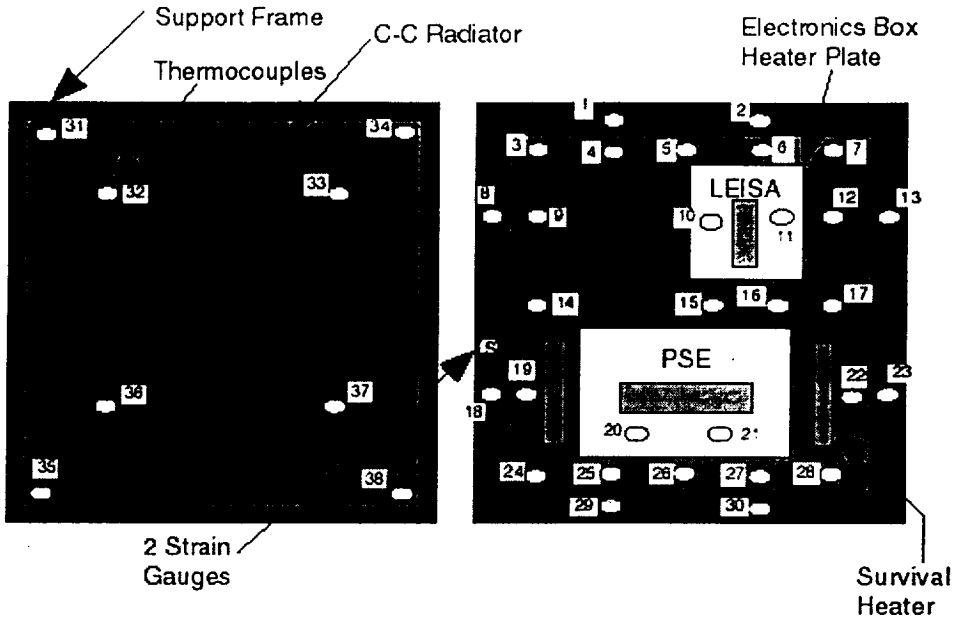

Figure 6: Thermocouple and Strain Guage Locations for the Carbon-Carbon Radiator Thermal Vacuum Test

The CCR is shown instrumented for thermal/vacuum testing and in the support frame in Figure 6. The two heater plates representing the electronics boxes and the survival heaters are attached to the backside (or inside) of the radiator. The LEISA plate is in the upper right, the PSE plate is in the lower center, and the two survival heaters are on both sides of the PSE plate. Also shown are the two plate heaters and the thermocouples that were used to monitor the temperature of the radiator during testing. The other side of the radiator is covered with silver teflon tape and will be exposed to space during the flight.

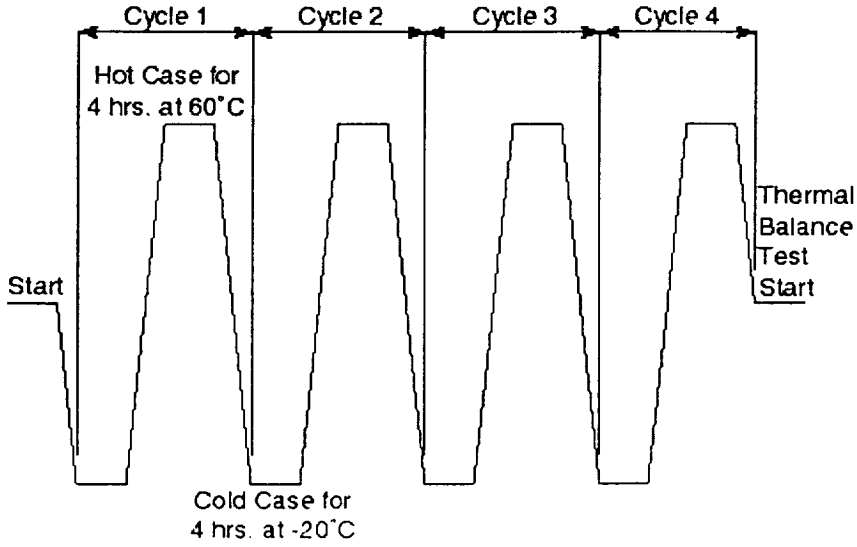

Figure 7: Thermal Test Cycles for the EO-1 C-C Radiator

The test fixture temperatures were recorded by a data acquisition system connected to a PC using Labview software. The temperatures were recorded throughout the entire test. The chamber pressure and the actual heater power were recorded. Type "T" thermocouples were used to monitor test temperatures. Thirty-eight were on the radiator and frame, and several were on the chamber wall, shroud, and platen. Two strain gauges were placed together on the outside surface of the support frame. See Figure 6 for rough thermocouple and strain gauge locations. Because the front side of the radiator was covered with silver teflon, the thermocouples were place on the heads of the attachment screws at the four corners and on screws in four of the GSE insert holes.

The tests were run with the heaters powered at various settings to provide a variety of differential temperature gradients across the panel. During the thermal cycle testing, there was no insulation on the radiator assembly, and the heaters were not used. The CCR was subjected to four cycles each consisting of a hot soak at 60°C for four hours and a cold soak at -20° C for four hours consistent with Figure 7. The chamber wall, shroud, and platen were controlled to a temperature that attained and sustained these desired conditions which were at least 10° C above and below the predicted flight temperatures.

During the thermal balance testing, the side of the radiator with the heater plates (interior surface) was insulated with a minimum of 5-layered MLI. The chamber walls, shroud, and platen were set to about -20°C (±5°C) during the testing. The heaters were set to the powers listed Table 2, and the radiator allowed to reach equilibrium. Once equilibrium was reached, the power was set for the next test. This pattern was repeated until all the tests were completed. Each test was considered complete when the temperatures reached steady state and changed less than ± 0.5°C in 30 minutes.

Table 2: Thermal Balance Test Conditions

No.	PSE Power(W)	LEISA Power(W)	Platen(°C)	Shroud(°C)
1	10	0	-20	-20
2	30	0	-20	-20
3	50	0	-20	-20
4	0	10	-20	-20
5	0	30	-20	-20
6	20	10	-20	-20
7	40	20	-20	-20
8	50	30	-20	-20

During the survival heater testing, the radiator was insulated as in the thermal balance test. The chamber walls, shroud, and platen were also set to the same temperatures as the thermal balance test. However, in the survival heater tests, the PSE and LEISA heaters were turned off, and the survival heaters were set to the input voltages listed in Table 3.

Table 3: Survival Heater Test Conditions

No.	Heater Voltage	Platen(C)	Shroud(C)
1	21	-20	-20
2	26	-20	-20
3	30	-20	-20
4	35	-20	-20

For all tests, the maximum heater surface temperature was not allowed to exceed 100°C, and the radiator temperature was held above -20°C. Throughout the thermal vacuum test, the chamber pressure was held at or below 5.0×10^{-5} Torr. The results of the above tests are presented and compared with the thermal model results in Section 3.3. The next section describes the thermal analysis.

2. Thermal Model

The thermal analysis was performed via a compilation of various software packages. The model geometry for the radiator itself (heater plates and frame included) was built in Femap 5.0. That geometry was then transferred to Thermal Synthesizer System (TSS). The TSS model consisted of both the radiator geometry (shown in Figure 8) and a mock cylindrical chamber to simulate the actual test chamber the experiment was performed in. The radiator was placed inside the chamber and closed to the ambient environment. Radiative couplings were then calculated using TSS. All objects were included in this calculation with exception to the honeycomb material and the cho-therm interface material adjacent to the heater plates. The treatment of the interface material will be dealt with later. A SINDA model was then created which consisted of all the conductive and radiative couplings within the system. Conductivity values used in the SINDA deck and optical properties used in the TSS radiative couplings determination are listed in Table 4.

Table 4: Component Physical Properties

Component	Material	Conductivity (W/m-K)	Emmisivity
Frame	Aluminum 6061	179.9	0.03
Radiator Heater Side	Carbon	200	0.80
Radiator Front Side	Carbon / Silver Teflon	200	0.81
Heater Plates	Aluminum 2024	121.1	- - -
MLI	7 mil Aluminized Mylar	- - -	0.78
Inner Chamber Surface	- - -	- - -	0.88
MLI / Heater Side Interface	- - -	- - -	0.03 – 0.01

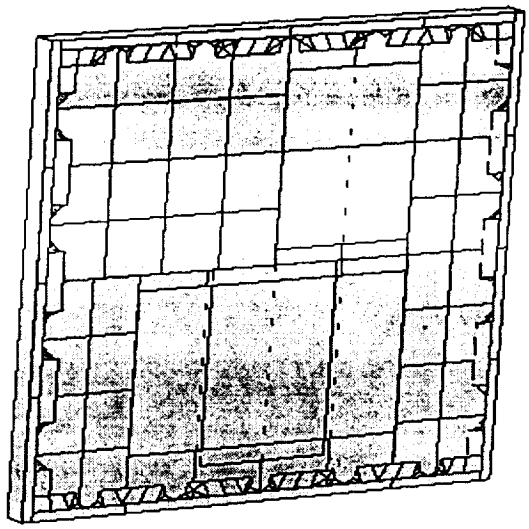

Figure 8: Carbon-Carbon Radiator Thermal Model, Heater Plate Side.

The radiator front is coated with silver teflon and radiates freely to space. The radiator back is the side which has the heater plates mounted on it. Note that the conductivities listed for the radiator front and back are planar values. SINDA model runs made were for a steady state case in order to simulate the thermal balance experiment. The model consisted of 275 nodes. Each face sheet was separated into 64 nodes (see Figure 8). The frame consisted of four parts. These were the perimeter (immediately adjacent to the interior honeycomb), the radiator front side frame flange, the radiator heater side flange, and the radiator heater side flange over-lapping the face sheets. Each side of the radiator frame, with exception to the portion of the heater side flange overlapping the heater side face sheets, was subdivided into four nodes.

Conductive couplings were taken between neighboring face sheet nodes on both sides of the radiator. Conductive couplings were also taken between the frame and the face sheet nodes that bound the frame. Couplings between the heater side face sheets and the overlapping frame were treated as conductance.

Group standard (GSFC Advanced Analytical Modeling Group) interface conductance values were used for the couplings between the heater plates and the cho-therm material, as well as the cho-therm and the radiator face sheet. The predominant mode of heat transfer between the face sheets, via the aluminum honeycomb, will be conduction. Radiation was neglected here. The relation used for the conductive coupling between adjacent face sheets (front to back) was taken from the Satellite Thermal Control Handbook[7], given as follows:

$$C_T = \left(\frac{8k\delta}{3S}\right)\left(\frac{LW}{T}\right)$$

where

$\delta = 0.0007''$ ribbon thickness

$S = 0.1875''$

L = height of area

W = width of area

T = through thickness of aluminum honeycomb

The thermal model is empirically designed around the thermal/vacuum test results. A total of nine heater dissipation configurations for the LEISA and PSE heaters were tested. A schematic of the thermocouple and heater locations for the front and heater side of the radiator is displayed in Figure 6. In the next section, the test results are presented, followed by the analysis results and comparisons between the two.

3. Results

Prior to the first test, the emissivities of the front and back of the radiator were measured. On the front (silver teflon), the emissivity was measured in five areas and averaged 0.81 overall. On the backside (box side), the emissivity was measured in three areas and averaged 0.80 overall. The temperatures of the front (TC 36) and back (TC 15) of the radiator, the platen (TC 56), and the shroud (TC 84) during the thermal cycle test are shown in Figure 9. Figure 10 shows the output of the two strain gauges and the temperature of the frame nearest the gauges (TC 18). The results of the thermal balance test are shown in Figure 11 and Figure 12. Figure 11 is a plot of the radiator front (TC 36) and back (TC 15), and the LEISA and PSE heater powers versus time. Figure 12 is a plot of the LEISA (TC11) and PSE (TC 20) temperatures and the heater powers.

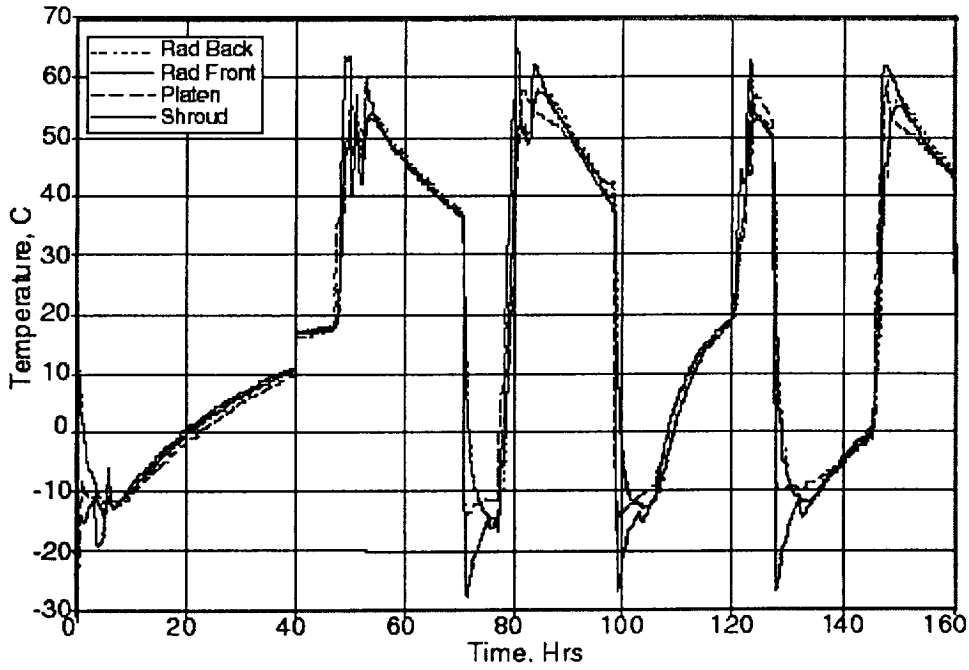

Figure 9: Thermal Cycles Test – Temperatures

Figure 13 and Figure 14 show plots of the temperatures of the back and front of the radiator and the survival heaters' power. The power to both heaters was measured as a single voltage and current. Figure 13 has the temperatures of the upper left (TC 3), upper right (TC 7), center (TC 15), lower left (TC 24) and lower right (TC 28) of the back or box side of the radiator. Figure 14 has the upper left (TC 31), upper right (TC 34), center (TC 36), lower left (TC 35) and lower right (TC 38) of the front or silver teflon side of the radiator. The temperatures at all of the locations on the back side of the CCR were measured with maximum power to the plates. These temperatures were compiled to generate the contour plot of temperature versus position on the panel shown in Figure 15.

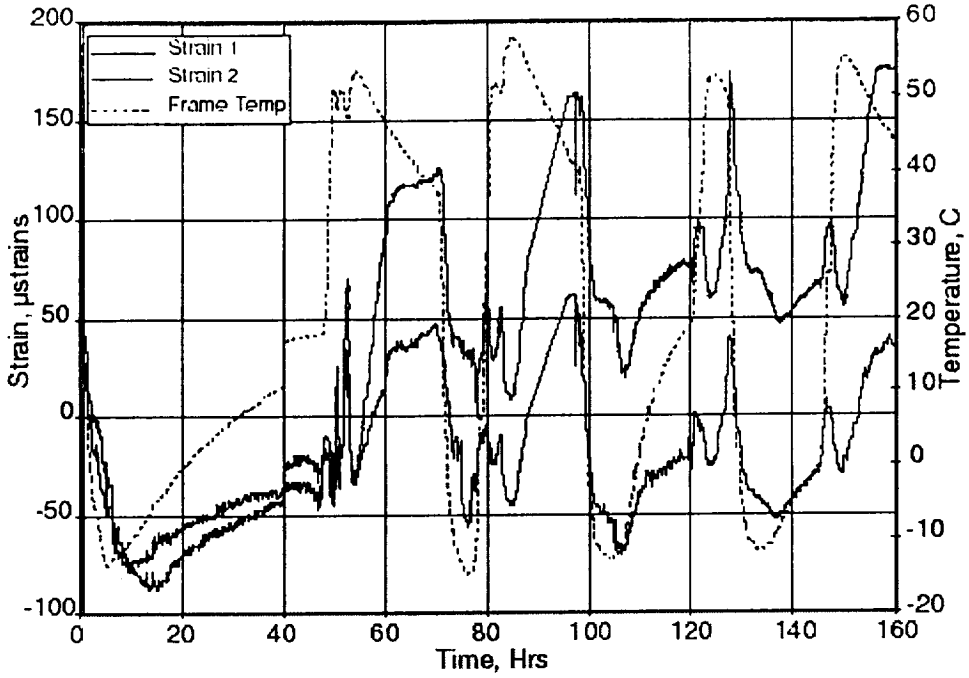

Figure 10: Thermal Cycles Test – Strain Gauges

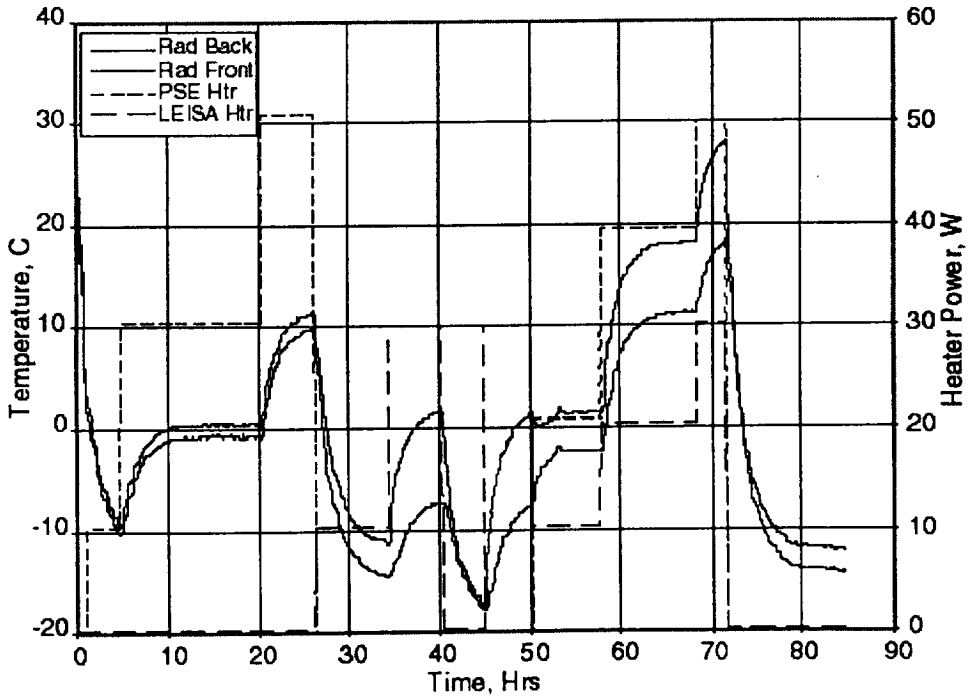

Figure 11: Thermal Balance Test – Radiator Temps & Heater Powers

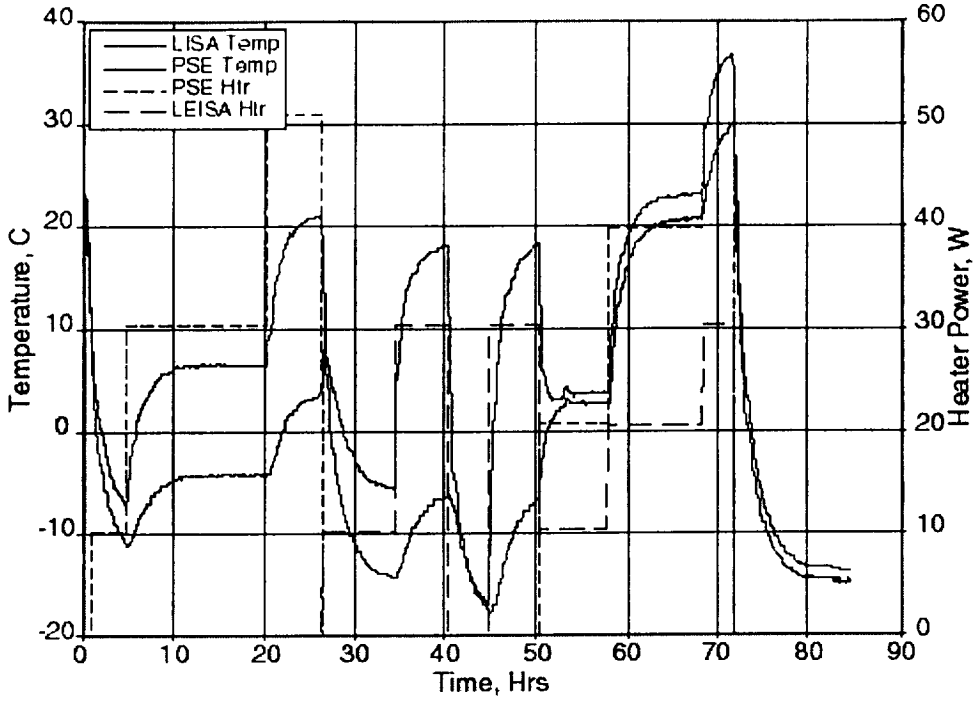

Figure 12: Thermal Balance Test – Plate Temps & Heater Powers

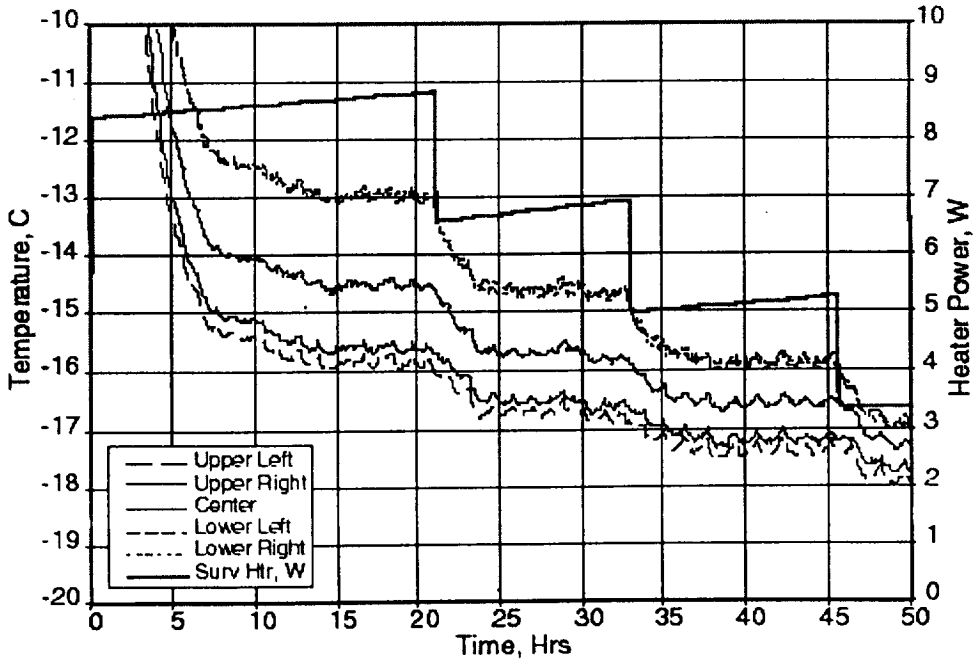

Figure 13: Survival Heater Test – Radiator Back

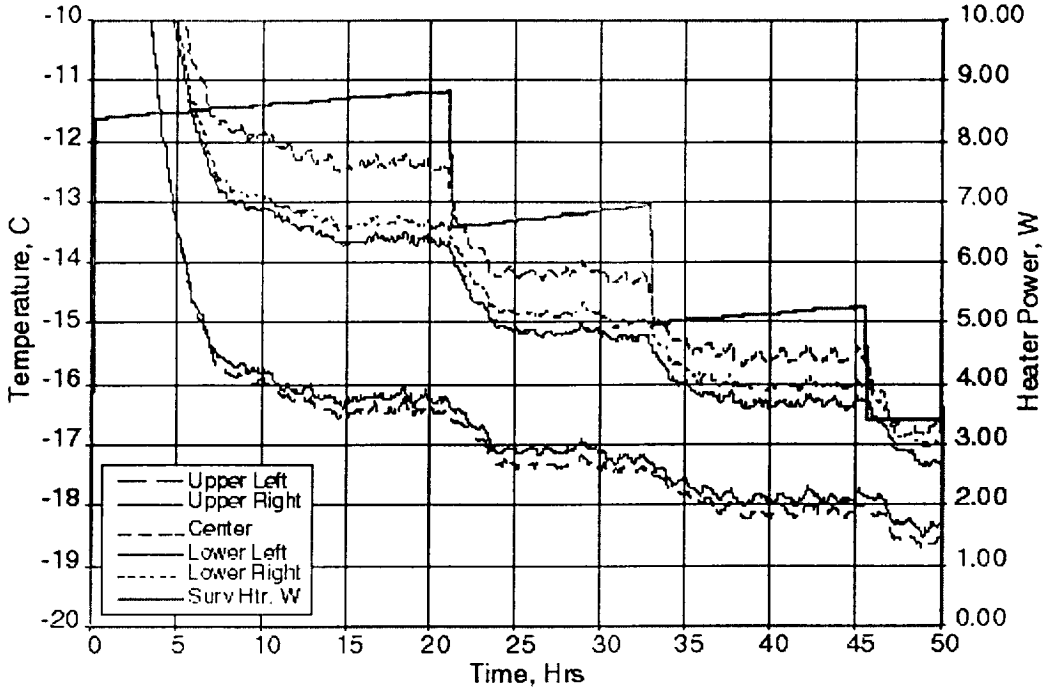

Figure 14: Survival Heater Test – Radiator Front

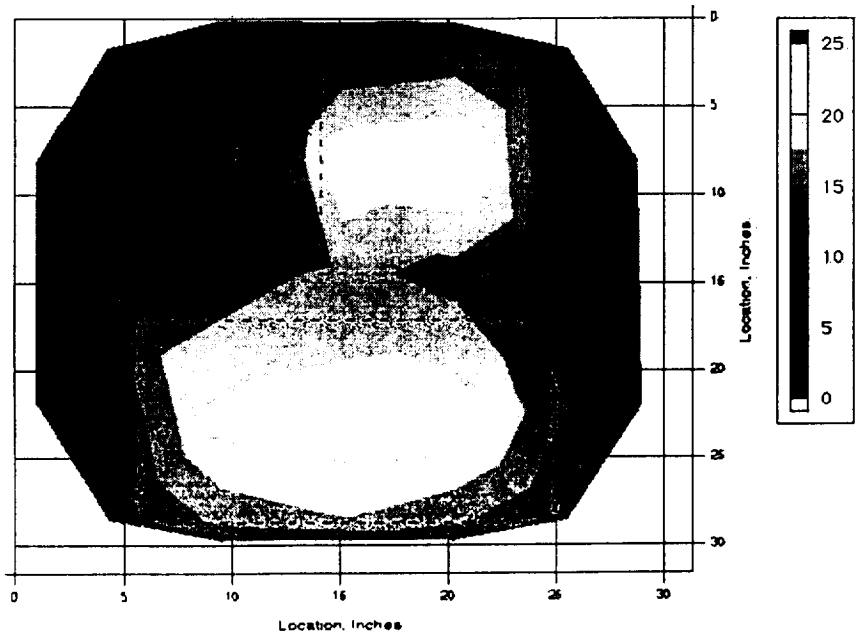

Figure 15: Back side of the CCR with maximum power to the plates.

Two test cases were selected for the thermal balance model/test comparison. These were the hot and cold extremes based on the sum heater wattage applied. They were as follows:

Table 5: Model Correlation Input Power

Case	LEISA Heater (Watts)	PSE Heater (Watts)
Cold	0	10
Hot	30	50

Heater plate temperatures were focused upon in the model design. The actual and theoretical test results for both cases were as follows:

Table 6: Theoretical and Experimental Heater Plate Temperatures

Heater	Cold Case Actual	Cold Case Analysis Model	Hot Case Actual	Hot Case Analysis Model
LEISA	-12	-15	37	35
PSE	-8	-10	30	32

(All temperature values presented here are in °C)

The model over-predicted the heater plate temperatures on the cold end by a nominal 3°C for both heaters. On the hot end, the model under-predicted the experiment by 2°C for the LEISA heater and over-predicted for the PSE heater by 1°C. A raw data plot of the heater powers and their corresponding temperatures for all nine configurations is displayed in Figure 11. Two thermocouples (one on each face side of the radiator) were tracked during the test. These were locations TC15 and TC36. Analysis model and experiment comparison results for these locations were as follows:

Table 7: Theoretical and Experimental Radiator Surface Temperatures

Location	Cold Case Actual	Cold Case Analysis Model	Hot Case Actual	Hot Case Analysis Model
TC15	-9	-11	28	30
TC36	-11	-13	18	18

(All temperature values presented here are in °C)

The analysis model over-predicted the heater plate temperatures on the cold end and the PSE temperature on the hot end. The LEISA plate temperature is under-predicted on the cold end by a few degrees. With regards to the TC locations, the model over predicts TC15's temperature in both the hot and cold case. TC36 is over predicted in the cold case and is approximately equal in the hot case. A raw data plot of these location temperatures and corresponding heater values for all nine configurations is displayed in Figure 12.

Please note that the initial model did not show the same degree of correlation with the experiment that the present model does. Variance occurred with temperature values for both the heater plates and face sheet TC locations. TC15 and TC36 both had fairly comparable values to the experimental data gathered for the hot case. However, the cold case for these two showed large discrepancies between the model and the physical data. The PSE and LEISA heater plates had the same temperature for the hot case and were off from the actual values by three and four degrees respectively. For the cold case, the temperature discrepancies enlarged. One trend noticed was that all the cold case temperatures for the analysis model were warmer than the actual values. In order for the model to foster the actual phenomenon more accurately, the performance band for all the temperatures on the plate would have to be expanded in the cold domain. There would also have to be a relaxation of the thermal coupling between the PSE and LEISA heaters on the hot end. This was approached through a variation of conductive and emissive parameters on the face sheets and the heaters. Conductance values between the heater plates and the cho-therm (interstitial material), as well as the cho-therm and the adjoining face sheets were varied. The effective emittance between the radiator's heater side (face sheets and heater plates) and the MLI was varied. The conductivity for the aluminum honeycomb was varied as well. Of all the parameters varied, the honeycomb conductivity was varied the most. All of the other parameters were simply tweaked. The parameters which radiator temperatures proved most sensitive to were the conductances between the cho-therm and the face sheets as well as the cho-therm and the heater plates. Since heating for the entire radiator came from the heater plates, the interstitial material joining the plates to the radiator face sheets was used as a retarding force to capture heat in the hot case, and to expel it more in the cold case. Variation of these parameters was ended upon finding a

combination suitable for comparison to the actual temperature values. Accuracy of the heater wattage applied for each case was also surveyed. Values yielded with the final combination were presented previously.

4. MECHANICAL PERFORMANCE

During launch of the EO-1 spacecraft, the CCR will be required to support the total (58 lb) weight of the boxes under an equivalent static load of 15 G's. The panel will also be required to react primary structural loads induced by the spacecraft bus. The first mode frequency of the panel and electronics box assembly, when attached to ground at the spacecraft mounting points, must exceed 100Hz. In flight, the panel must react to forces resulting from the CTE mismatch between the carbon-carbon facesheet and on-orbit temperature variations in the range of -10° to +50° C. In this work, the panel was analyzed to -20° to +60° C.

The CCR and electronics box assembly was subjected to vibration testing in the three primary axes to assess the mechanical performance of the CCR. Strain gauges were also used in the thermal cycle tests mentioned in Section 3 to monitor the forces induced by the thermal mismatch between the CCR and the support frame, which simulated the stiffness of the spacecraft. GSFC personnel inspected the panel visually and by non-destructive evaluation after each test. Finite element models of the panel assembly and hand calculations were used as needed to predict the first mode frequency and compute margins of safety to ensure the CCR could withstand the anticipated structural loads. Descriptions of the mechanical tests are presented in the next three sections, which are followed by descriptions of the finite element models. Subsequently, results from the environmental tests, inspection, and analysis are presented and compared.

1. Vibration Testing

The purpose of the vibration testing was to qualify the CCR for flight on the EO-1 spacecraft by applying a sine burst input of 18.8 G's, which is 1.25 times the limit load of 15G's specified by the spacecraft integrator, Swales Aerospace Inc. (SAI). The tests were also used to verify that the panel and box assembly meets the minimum stiffness requirement specified by SAI.

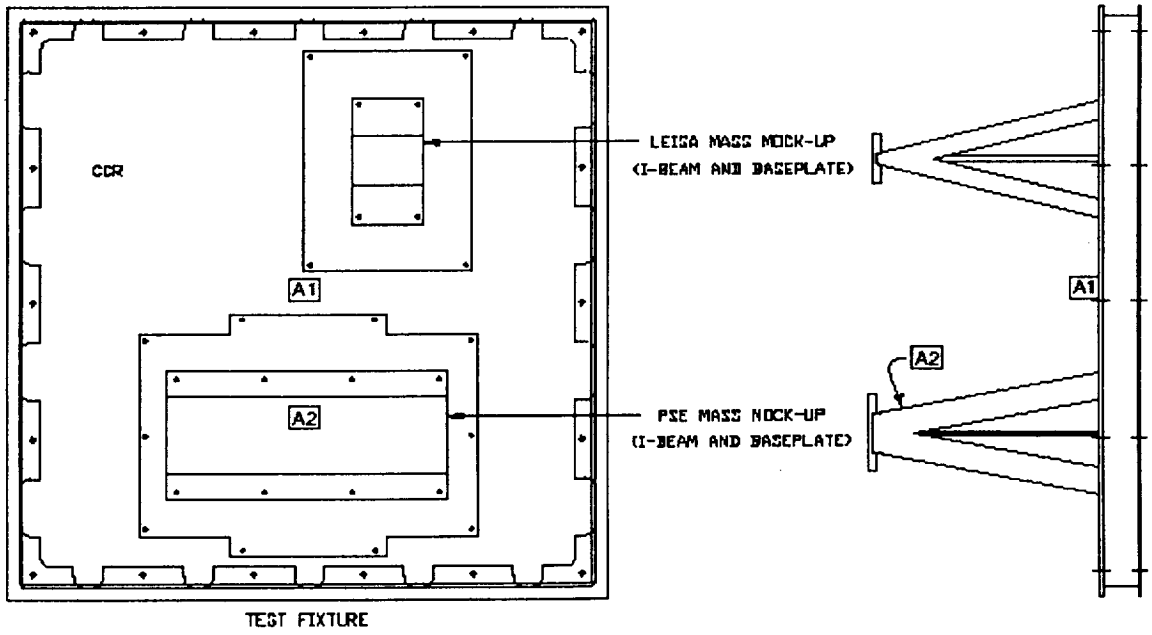

Figure 16: Vibration Test Configuration

The test article consisted of the flight CCR, mass mockups and base plates representing the PSE and LEISA/AC electronics boxes, and a test frame used to mount the CCR to the shaker table. The test configuration is shown in Figure 16. The weight of the PSE and LEISA/AC mass mockups were approximately 44 and 11 pounds respectively. The total weight of the test article was 68 lbs. Testing was performed in the GSFC Vibration Facility using two LING/MB C-220 exciters. For the Z-axis test, the test article was mounted to the head expander of exciter #1 using a test plate. The X and Y-Axis testing was performed using exciter #2 with the test article mounted to the slip table using the same test plate. Instrumentation during the vibration testing consisted of two in-axis control accelerometers on the test plate and two triaxial response accelerometers mounted on the test article. The locations of the response accelerometers (A1 and A2) are shown in Figure 16. Accelerometer

A1 was placed on the CCR near the midpoint and accelerometer A2 was placed near the top on the web of the PSE mass mock-up I-beam.

For each axis a series of base excitations were applied to the test article. First, a low-level signature sine sweep of 0.25 G was applied from 15 to 200 Hz at a rate of 2 octaves/minute. This was followed by a sine burst of 18.8 G at 22.5 Hz for 5 cycles. Next, the low-level sine sweep was repeated. At each step the data obtained from the respective base excitation was studied for anomalies prior to proceeding to the next test axis. In particular, the data from the control channels for the full level sine burst were examined to verify that the proper input levels had been achieved. The data obtained from the pre and post sine sweeps were plotted, and overlaid to check for any potential changes in resonances induced by test article or fixture failure. The results of the vibration tests are presented later.

In addition to the vibration testing, the thermal cycling tests were used to qualify the CCR for flight on EO-1. The mechanical details of this test are discussed in the next section. The vibration testing results are presented after the details of the thermal testing, mechanical inspection, and mechanical model are presented.

2. Thermal Cycle Testing

The thermal cycle testing described in Section 3.0 also served as an important structural test. In this test, the CCR, which has a very low CTE, is attached to an aluminum frame, which has a relatively high CTE. As a bulk temperature change is applied to the assembly the frame will tend to expand or contract more than the CCR, resulting in potentially significant forces. These forces were monitored during the thermal cycle test by applying two strain gauges to the test frame.

Specifically for the purpose of this test, the stiffness of the frame was designed to match the spacecraft in the plane of the CCR. The basic design of the test frame is a C-channel surrounding the CCR. The neutral axis of the C-channel was aligned with the mid-plane of the CCR to avoid any unanticipated moments. The strain gauges were affixed to the web of the C-channel and the primary axes of the gauges were aligned with the long axis of the C-channel. Each gauge was located the same distance from the corner of the frame, and one was located near the top and bottom corners of the C-channel cross-section. This provided for two measurements of the axial strain in the long dimension of the C-channel. From these measurements, the axial force and moment in the frame, and hence load on the CCR could be determined. These results are presented later.

As the CCR progressed through the mechanical tests, it was monitored for failure. The approaches used to monitor for failure are discussed in the following section.

3. Inspection

In addition to the pre and post sign sweep comparisons mentioned in Section 4.1, the panel was visually inspected for damage. Radiographic Non-Destructive Evaluation (NDE) was also conducted on the CCR. GSFC personnel performed non-destructive radiography at the panel and box insert corner locations on four occasions during the testing sequence. Radiographs were obtained before the start of testing, after thermal testing, and twice after vibration testing. All except the third set of radiographs (after vibration testing) were taken of the panel without the attached frame and baseplates. For the third set, the frame and baseplates were left attached to the panel with the fasteners fully torqued. Each set of images were compared and studied for differences due to structural failure. The results of the inspection are discussed later.

4. Structural Model

A UAI/NASTRAN finite element model of the panel hard mounted at the spacecraft attachment points was developed using SDRC/I-DEAS to predict the fundamental frequencies (see Figure 4a). The model included the attached LEISA and PSE boxes modeled as concentrated masses attached at the 14 interior insert locations. This model corresponds with case B in Table 1. Similar models of the panel attached to the test frame with rigid boxes (case C in Table 1), and of the panel attached to the test frame with aluminum base plates (case D in Table 1 and shown in Figure 4b) were also developed. In all cases the honeycomb panel was modeled using QUAD4 elements with an equivalent cross section. Linear spring elements were placed between the panel and the attachment points to account for the added compliance of the potting compound. The spring stiffnesses specified by LMVS were 12.6e4 lb/in in-plane and 6.59e4 lb/in normal to the panel surface. MR&D specified the following effective Carbon-Carbon facesheet properties:

Table 8: Carbon-Carbon Composite Facesheet Effective Properties

Material Properties		Material Allowables	
$E_1 = E_2 =$	1.62e7 psi	$S_1^T = S_2^T =$	30.7e3 psi
$G_{12} =$	6.11e6 psi	$S_3^T =$	1.0e3 psi
$G_{1Z} = G_{2Z} =$	0.35e6 psi	$S_1^C = S_2^C =$	12.7e3 psi
$\nu_{21} = \nu_{12} =$	0.32	$S_3^C =$	6.0e3 psi
$\alpha_1 = \alpha_2 =$	-1.182e-6 1/(°C)	$T_{23} = T_{13} =$	1.4e3 psi
		$T_{12} =$	10.0e3 psi

GSFC standard factors of safety of 1.25 and 1.4 were used on yielding and ultimate failure, respectively. Stresses exceeding the proportional limit of the carbon-carbon composite material were considered as ultimate failure. Margins of safety were computed based on the following equation:

$$\text{M.S.} = \frac{\sigma_{\text{allow}}}{\sigma_{\text{calc}}(\text{F.S.})} - 1$$

The initial EO-1 CCR design was modified due to substantial changes to the spacecraft design. MR&D[6] completed a trade study for the facesheet design prior to this design change. The results are presented in Ref. 6. NASA/GSFC completed an analysis of the MR&D recommended design for the new requirements specified by SAI[1]. LMVS[8] completed the design and analysis of the inserts common to the CCR for the flight application. The following sections are a summary of the results from the GSFC and LMVS analyses.

The CCR will experience the 15g inertial loading during launch and the thermal loads on orbit. Consequently, these load cases were analyzed separately. A UAI/NASTRAN finite element model simulating the 15g-acceleration load in all directions on the panel and box assembly attached to ground was used to compute the stresses in the composite facesheets and honeycomb core. In-plane running loads specified by SAI were added to the finite element stresses. The transverse shear computed from the above finite element model due to the 15g acceleration and the spacecraft running loads were summed. The analysis assumed that the honeycomb core carried these loads.

In a similar fashion, margins of safety for a bulk temperature change of 40° C from ambient were computed using a finite element model of the CCR assembly attached to an aluminum frame shown Figure 4b. The aluminum frame was designed to simulate the in-plane stiffness of the spacecraft. The stiffnesses of the boxes were simulated with solid aluminum plates. Hand calculations were used to compute the margins of safety for the perimeter and box fasteners for both the inertial and thermal load cases in conjunction with a 38 in-lb preload specified by SAI.

5. Results

The CCR was sine burst tested to 18.8 G (1.25 x 15 G) in all three axes, and was accompanied by pre and post low-level sine sweeps in accordance with Section 4.1. The first mode frequency of the test configuration was 89 Hz. The first mode frequency predicted by finite element analysis of the test configuration (case C in Table 1) was 93 Hz. The analysis of the CCR and box assembly attached to ground predicted a first mode frequency of 112 Hz. The model and test results are within 5%. This provides some validation of the CCR finite element model, and indicates that the first mode frequency of 112 Hz computed using the panel hard mounted at the spacecraft attachment points configuration is reliable.

For all three axes, the test data showed that the sine burst input level of 18.8 G's was achieved. Low level signature sweeps performed before and after the sine burst testing in each axis showed that there were no significant changes in the resonant frequencies of the test article. In addition, radiographic inspection of insert locations was performed before and after sine burst testing consistent with Section 4.3. The inspection examined inserts at the four corners of the panel as well as the corner inserts of the box mounting locations. The results of the inspection indicated no change to either the potting compound or the surrounding honeycomb core at those locations as a result of the test. Consequently, the panel survived the sine burst loads, which indicates that there are positive margins on the acceleration loads.

The CCR was subjected to thermal cycling in accordance with Sections 3.0 and 4.2. An aluminum frame simulating the EO-1 spacecraft stiffness in the plane of the panel was attached to the CCR during thermal testing. Two strain gauges were placed on the frame near the top and bottom of the "C" cross section of the frame. The strains were recorded during thermal cycling and are shown in Figure 10. The frame was also subjected to a thermal cycle with the CCR removed for calibration. The resulting free strains were subtracted from the strains recorded while the CCR was attached to the frame.

The peak value of adjusted strain was approximately 150 μ. Strains were also obtained from the finite element analysis of the thermal test configuration (case D in Table 1) at the locations of the strain gauges. The peak finite element strain was approximately 300 μ, which indicates that the apparent loads during thermal cycling were approximately half the loads predicted by the finite element model. This implies that the system is overall more compliant than predicted, and the finite element results are conservative. The finite element loads were used to compute the margins of safety presented, and as such, the margins of safety are conservative. The above difference in strain most likely occurs because the clearance between the insert through hole and the fastener diameters was not included in the finite element model. As a result there was frictional sliding between the CCR and frame during the test. There is evidence of this behavior in Figure 10.

Radiographic inspection of the radiator and box corner inserts was also completed before and after the thermal testing. No differences were found between the NDE images taken before and after the thermal testing. The above NDE showed that strength testing did not damage the CCR. As such, the panel survived the proof loads and is qualified for flight. This also validates that there are positive margins on the acceleration and thermal loads, which provides some validation of the positive margins mentioned in this report.

Finite element and hand analyses were used to compute margins of safety for the radiator facesheets, honeycomb core, fasteners, and insert potting compound. The margins of safety were determined to be positive in all cases for loads induced by both the 15 G inertial load and 40°C change in temperature.

5. CONCLUSIONS

Thermal/vacuum and vibration testing of the EO-1 CCR were successfully completed at GSFC. Thermal and structural analyses were also completed at GSFC and showed reasonable correlation with the test results. The thermal model temperature predictions on the heater plates and face sheets were shown to be within a couple of degrees of the experimental results. The thermal vacuum testing and this model correlation activity provides validation of the thermal performance of the C-C radiator for use on the EO-1 Spacecraft. The model will also be used to correlate the on-orbit data from the S/C to provide validation of the technology in flight applications. Mechanical analysis showed that the CCR meets the stiffness requirement. Stress analysis also showed positive margins for all load conditions specified by SAI. Radiographic inspection of critical insert locations, before and after testing, showed no change in the CCR microstructure, vibration sine sweeps showed no change in the CCR resonance characteristics, and visual inspection revealed no apparent damage. Therefore, the CCR has been shown, through analysis and testing, to meet or exceed all launch and on-orbit performance requirements specified by SAI and is fully qualified for flight on the EO-1 spacecraft.

Here we note that the thermal requirements of this particular application fall below the capability of the carbon-carbon material. At the same time the structural requirements are relatively demanding. There is little doubt as to the thermal capability of carbon-carbon, but structural applications of this type have been uncommon to date. This work provides experience in using the material for structural applications and demonstrates carbon-carbon as a viable option for both thermally and structurally demanding design applications. As mentioned above, the radiator exceeded the performance expectations, and in some regards may have been overdesigned. In future applications, the authors believe more design iterations and testing could yield improved thermal to weight ratios at reduced cost.

6. ACKNOWLEDGMENTS

The authors gratefully acknowledge the effort of GSFC personnel that supported this effort. In particular: Scott Gordon, Gurnie Hobbs, Mario Martins, and Brad Parker.

7. REFERENCES

1. P. Alea. Swales Aerospace Inc., Beltesville, MD.
2. H.G. Maahs, W.L. Vaughn, and W. Kowbel. "Four Advances in Carbon-Carbon Materials Technology." The Fourth National Technology Transfer Conference & Exposition. December 7-9, 1993, CA.
3. BFGoodrich Company, Santa Fe Springs, CA.
4. W.L. Vaughn. "Carbon-Carbon Composite Facesheet Mechanical Characterization for the EO-1 Bay Four Radiator." NASA/TM-98-0000.
5. W. Vaughn, E. Shinn, S. Rawal, and J. Wright. "Carbon-Carbon Composite Radiator Development for the EO-1 Spacecraft."
6. B.J. Sullivan, G.F. Jones, K.W. Buesking, and M.J. Dunn. "Carbon-Carbon Space Radiator Program Material Trade Study and Design Task." Materials Research & Design, Inc. Rosemont, PA. WL-SASHM-69-1.
7. D. Gilmore, 1994, *Satellite Thermal Control Handbook*, The Aerospace Corporation Press, El Segundo, CA.
8. J. Wright. Lockhead Martin Voight Systems, Dallas, TX.
9. S. Rawal. Lockhead Martin Astronautics, Denver, CO.